ON THE APPLICATION OF FOURIER ANALYSIS TO REGULAR AND CHAOTIC DYNAMICS OF RECTANGULAR FLEXIBLE PLATES SUBJECTED TO SHEAR-HARMONIC LOADING

Awrejcewicz J. [1] , Papkova I.V. [2] , Krylova E.U. [2] , Krysko V.A. [2]

[1] *The Technical University of Lodz, Department of Automation and Biomechanics, 1/15 Stefanowskiego St., 90-924 Lodz, Poland.* awrejcew@p.lodz.pl

[2] *The Saratov State Technical University, Department of Mathematics and Modeling, Polytechnical 77, 410054 Saratov, Russia.* tak@san.ru

SUMMARY: Non-linear dynamics of flexible rectangular plates subjected to external shear-harmonic load action is investigated. It is shown that the application of the classical and widely used Fourier analysis does not allow us to obtain a real picture of the frequency vibration characteristics in every time instant. On the other hand, the application of the wavelets approach enables us to follow frequency time evolutions. Our numerical results indicate that vibrations in different plate points occur with the same frequencies set although their power is different. Hence, the vibration characteristics can be represented by one arbitrarily taken plate point. Scenarios of transitions from regular to chaotic dynamics are illustrated and discussed including two novel scenarios not reported so far in the existing literature.

KEYWORDS: chaotic dynamics, wavelets, plates

1. INTRODUCTION

Plates are widely applied in various branches of industry like aviation, ship construction, civil engineering, etc. Since the plate-members of constructions are in general subjected to the action of various loading, they need careful modeling and validated numerical investigations. Today's industrial needs are mainly focused on the choice of parameters of the analyzed construction to keep it working in safe regimes. Continual systems such as plates have been analyzed from the point of view of chaotic dynamics in references [1-2]. Being in many cases very dangerous for constructions, chaotic dynamics was detected in fluid mechanics relatively long ago, while chaos exhibited by plates and shells have been studied just recently [3-11]. The aim of our contribution is to study chaotic vibrations of flexible rectangular plates subjected to shear loading harmonic action, which belongs to novel and challenging open problems.

2. GOVERNING EQUATIONS

A plate with constant stiffness and density within a classical non-linear theory subjected to the action of harmonic shear loading is considered. In the initial time interval $t \in [0;1]$ a small static transversal load is applied. In 3D co-ordinates the investigated plate can be represented in the following form:

$$\Omega = \{x_1, x_2, x_3 \mid (x_1, x_2) \in [0;a] \times [0;b], x_3 \in [-h;h]\}\ ,\ 0 \le t < \infty\ .$$

The following non-dimensional PDEs governing dynamics of the shallow shells are studied:

$$\frac{1}{12(1-\mu^2)}\left(\nabla_\lambda{}^4 w\right) - L(w,F) + \frac{\partial^2 w}{\partial t^2} + \varepsilon\frac{\partial w}{\partial t} - q(x_1,x_2,t) + 2S\frac{\partial^2 w}{\partial x \partial y} = 0,$$
$$\nabla_\lambda{}^4 F + \frac{1}{2}L(w,w) = 0, \tag{2.1}$$
$$\nabla_\lambda{}^4 = \frac{1}{\lambda^2}\frac{\partial^4}{\partial x_1{}^4} + \lambda^2\frac{\partial^4}{\partial x_2{}^4} + 2\frac{\partial^4}{\partial x_1{}^2 \partial x_2{}^2},$$
$$L(w,F) = \frac{\partial^2 w}{\partial x_1{}^2}\frac{\partial^2 F}{\partial x_2{}^2} + \frac{\partial^2 w}{\partial x_2{}^2}\frac{\partial^2 F}{\partial x_1{}^2} - 2\frac{\partial^2 w}{\partial x_1 \partial x_2}\frac{\partial^2 F}{\partial x_1 \partial x_2},$$

where w and F are the functions of deflection and stress, respectively. System (2.1) is reduced to a non-dimensional form using the following non-dimensional parameters: $\lambda = a/b$, $x_1 = a\bar{x}_1$, $x_2 = a\bar{x}_2$, $w = 2h\bar{w}$ denotes deflection; $F = E(2h)^3\bar{F}$ is the stress function; $t = t_0\bar{t}$ denotes time; $q = \frac{E(2h)^4}{a^2b^2}\bar{q}$ is the external loading; $\varepsilon = (2h)\bar{\varepsilon}$ is the damping coefficient of a surrounding medium, and $S = \frac{E(2h)^3}{ab}\bar{S}$ is the external shear loading. Bars over the non-dimensional parameters are omitted. Furthermore, the following notations are introduced: a, b denote plate length regarding x_1 and x_2, respectively, and μ is the Poisson coefficient.

The following boundary conditions are attached to equations (2.1):

1. Support on flexible non-stretched (non-compressed) ribs

$$w = 0,\ \frac{\partial^2 w}{\partial x_1{}^2} = 0;\quad F = 0,\ \frac{\partial^2 F}{\partial x_1{}^2} = 0 \text{ for } x_1 = 0;1;\ w = 0,\ \frac{\partial^2 w}{\partial x_2{}^2} = 0,\quad F = 0,\ \frac{\partial^2 F}{\partial x_2{}^2} = 0 \text{ for } x_2 = 0;1. \tag{2.2}$$

2. Clamping on a contour

$$w = 0,\ \frac{\partial w}{\partial x_1} = 0;\quad F = 0,\ \frac{\partial F}{\partial x_1} = 0 \text{ for } x_1 = 0;1;\ w = 0,\ \frac{\partial w}{\partial x_2} = 0;\quad F = 0,\ \frac{\partial F}{\partial x_2} = 0 \text{ for } x_2 = 0;1. \tag{2.3}$$

3. Free support on a contour

$$w = 0,\ \frac{\partial^2 w}{\partial x_1{}^2} = 0;\quad F = 0,\ \frac{\partial F}{\partial x_1} = 0 \text{ for } x_1 = 0;1;\ w = 0,\ \frac{\partial^2 w}{\partial x_2{}^2} = 0;\quad F = 0,\ \frac{\partial F}{\partial x_2} = 0 \text{ for } x_2 = 0;1. \tag{2.4}$$

4. Clamping with flexible non-stretched (non-compressed) ribs

$$w = 0,\ \frac{\partial w}{\partial x_1} = 0;\quad F = 0,\ \frac{\partial^2 F}{\partial x_1{}^2} = 0 \text{ for } x_1 = 0;1;\ w = 0,\ \frac{\partial w}{\partial x_2} = 0;\quad F = 0,\ \frac{\partial^2 F}{\partial x_2{}^2} = 0 \text{ for } x_2 = 0;1. \tag{2.5}$$

The following initial conditions are applied

$$w(x_1,x_2)\big|_{t=0} = 0,\ \frac{\partial w}{\partial t} = 0. \tag{2.6}$$

3. FINITE DIFFERENCE METHOD (FDM)

In what follows, we consider the Finite Difference Method with approximation $O(h^2)$ regarding spatial coordinates x_1 and x_2. In this case an application of the FDM to the infinite system of degrees-of-freedom governed by PDEs (2.1) yields a finite lumped system governed by the following difference-operator equations

$$
\begin{aligned}
&-\frac{1}{12(1-\mu^2)}\left(\lambda^{-2}\Lambda_1^2 w_{ij}+2\Lambda_{12}^2 w_{ij}+\lambda^2\Lambda_2^2 w_{ij}\right)-\Lambda_1 w_{ij}\cdot\Lambda_2 F_{ij}-\Lambda_2 w_{ij}\cdot\Lambda_1 F_{ij}+\Lambda_{12} w_{ij}\cdot\Lambda_{12} F_{ij}+\\
&+q_i-P_x\Lambda_2-P_y\Lambda_1-2S\Lambda_{12}=\left(w_{tt}+\varepsilon w_t\right)_{i,j}\\
&\left(\lambda^{-2}\Lambda_1^2 F_{ij}+2\Lambda_{12}^2 F_{ij}+\lambda^2\Lambda_2^2 F_{ij}\right)=-\Lambda_1 w_{ij}\cdot\Lambda_2 w_{ij}+\left(\Lambda_{12} w_{ij}\right)^2,\\
&\Lambda_i y=\frac{1}{h_i^2}\left[y\left(x_i-h_i\right)-2\cdot y\left(x_i\right)+y\left(x_i+h_i\right)\right],\ i=1,\,2,\\
&\Lambda_{12} y=\frac{1}{4h_1h_2}\left[y\left(x_1+h_1,x_2+h_2\right)+y\left(x_1-h_1,x_2-h_2\right)-\left(x_1+h_1,x_2-h_2\right)-\left(x_1-h_1,x_2+h_2\right)\right],\\
&\Lambda_i^2 y=\frac{1}{h_i^4}\left[y\left(x_i-2h_i\right)-4y\left(x_i-h_i\right)+6y\left(x_i\right)-4y\left(x_i+h_i\right)+y\left(x_i+2h_i\right)\right],\ i=1,\,2,\\
&\Lambda_{12}^2 y=\frac{1}{h_1^2h_2^2}\left[y\left(x_1-h_1,x_2-h_2\right)-2y\left(x_1-h_1,x_2\right)+y\left(x_1-h_1,x_2-h_2\right)-2\left(x_1,x_2-h_2\right)+\right.\\
&\left.4y\left(x_1,x_2\right)-2y\left(x_1,x_2+h_2\right)+y\left(x_1+h_1,x_2-h_2\right)-2\left(x_1+h_1,x_2\right)+y\left(x_1+h_1,x_2+h_2\right)\right]
\end{aligned}
\tag{3.1}
$$

The following initial conditions are attached to system (3.1):

$$
w_{ij}=f_1(x_{1k},\ x_{2k}),\ w_n'=f_2(x_{1k},x_{2k}),\ (0\le k\le n),\ 0\ \le\ t\ <\ \infty\ ,
$$

whereas the boundary value conditions are formulated in the following form:

1. Free support on a contour

$$
\begin{aligned}
&w_{n,j}=0,\ \ w_{n,j}=-w_{n-2,j},\ F_{n,j}=0,\ F_{n,j}=-F_{n-2,j},\quad j=1,\,...,m-1,\\
&w_{i,m}=0,\ \ w_{i,m}=-w_{i,m-2},\ F_{i,m}=0,\ F_{i,m}=-F_{i,m-2},\quad i=1,\,...,n-1.
\end{aligned}
\tag{3.2}
$$

2. Clamping on a contour

$$
\begin{aligned}
&w_{n,j}=0,\ \ w_{n,j}=w_{n-2,j},\ F_{n,j}=0,\ F_{n,j}=F_{n-2,j},\quad j=1,\,...,m-1,\\
&w_{i,m}=0,\ \ w_{i,m}=w_{i,m-2},\ F_{i,m}=0,\ F_{i,m}=F_{i,m-2},\quad i=1,\,...,n-1.
\end{aligned}
\tag{3.3}
$$

3. Support on flexible non-stretched (non-compressed) ribs

$$
\begin{aligned}
&w_{n,j}=0,\ \ w_{n,j}=-w_{n-2,j},\ F_{n,j}=0,\ F_{n,j}=F_{n-2,j},\quad j=1,\,...,m-1,\\
&w_{i,m}=0,\ \ w_{i,m}=-w_{i,m-2},\ F_{i,m}=0,\ F_{i,m}=F_{i,m-2},\quad i=1,\,...,n-1.
\end{aligned}
\tag{3.4}
$$

4. Clamping with flexible non-stretched (non-compressed) ribs

$$
\begin{aligned}
&w_{n,j}=0,\ \ w_{n,j}=w_{n-2,j},\ F_{n,j}=0,\ F_{n,j}=-F_{n-2,j},\quad j=1,\,...,m-1,\\
&w_{i,m}=0,\ \ w_{i,m}=w_{i,m-2},\ F_{i,m}=0,\ F_{i,m}=-F_{i,m-2},\quad i=1,\,...,n-1.
\end{aligned}
\tag{3.5}
$$

The system of equations (3.1) – (3.5) is solved via the fourth-order Runge-Kutta method, where on each time step a large system of algebraic linear equations is solved. The Runge principle allows us to choose a time step properly.

3.1. Validity and convergence of results

We consider a rectangular plate with homogeneous boundary conditions (3.2) and the initial conditions $f_1(x_{1k},\ x_{2k})=0,\ f_2(x_{1k},x_{2k})=0$ being subjected to the action of a shear-harmonic load in the form of $S=s_0\sin\omega_p t$, where ω_p and s_0 are the frequency and amplitude of the external excitations, respectively. Damping coefficient $\varepsilon=1$, whereas Poisson's coefficient $\mu=0.3$. We investigate numerically a convergence of the FDM versus a number n of partition of intervals $[0;\,1]$ and $[0;\,1]$ of the rectangular plate in regular (periodic) and chaotic regimes.

Let us study first the point $A(s_{01},\omega_1)=A(8.6,13.4)\in\{s_0,\omega_p\}$ belonging to a periodic zone. Three curves for $n=m=12,\ 14,\ 16$ are reported in Figure 1. Increasing n causes initially a decrease of the output signals amplitude, whereas for $n=m=14,\ 16$ the curves fully overlap.

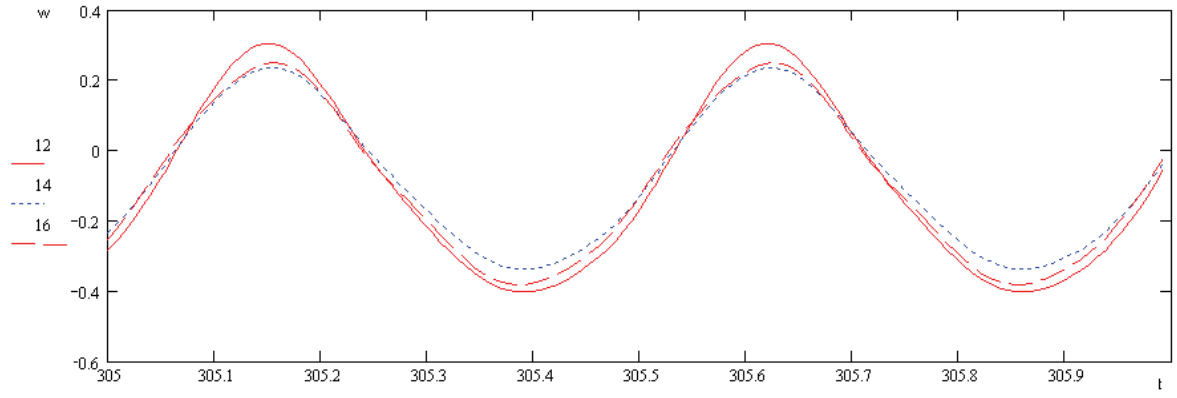

Figure 1 - Deflection $w(t)$ versus n in a periodic zone

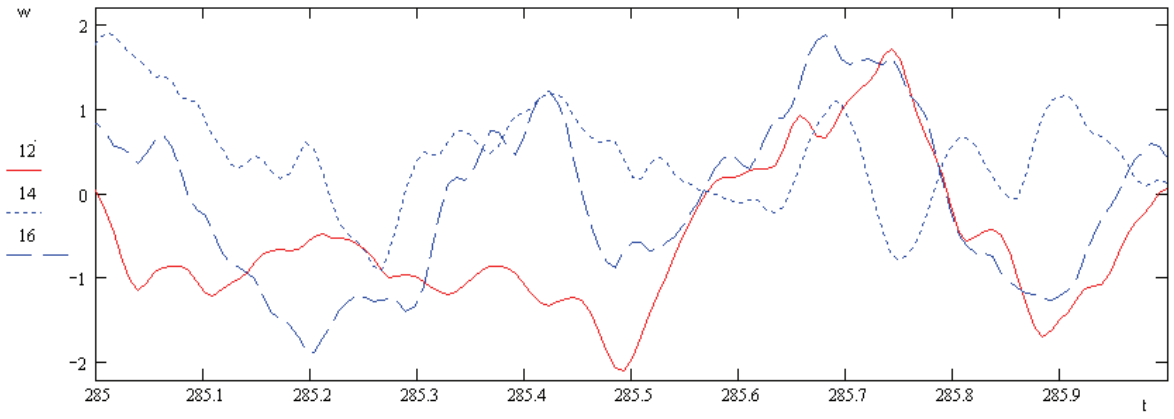

Figure 2 - Deflection $w(t)$ versus n in a chaotic zone

Let us consider one more point $B(s_{02},\omega_1) = B(28.7,13.4) \in \{s_0,\omega\}$, but in a chaotic zone. For all $n = 12, 14, 16$ the studied signals differ from each other (see Figure 2).

In what follows, we study convergence of the FDM with respect to computation of the Lyapunov exponents. For this purpose we monitor evolution of the Lyapunov exponents with time ($280 \le t \le 285$) for a number of partitions ($n = 12, 14, 16$) in periodic and chaotic zones. In point $A(s_{01},\omega_1) = A(8.6,13.4) \in \{s_0,\omega_p\}$ the Lyapunov exponents for all studied partitions are negative, which indicates that in the investigated point ($A(s_{01},\omega_1) = A(8.6,13.4) \in \{s_0,\omega_p\}$) vibrations are periodic (Figure 3).

On the other hand, in the point $B(s_{02},\omega_1) = B(28.7,13.4) \in \{s_0,\omega\}$ the Lyapunov exponents for all partition numbers are positive, which proves that chaos occurs in this point (Figure 3).

Let us construct a wavelet spectrum for the points $A(s_{01},\omega_1) = A(8.6,13.4) \in \{s_0,\omega\}$ and $B(s_{02},\omega_1) = B(28.7,13.4) \in \{s_0,\omega\}$ for different numbers of partition ($n = 12, 14, 16$) in the governing equations (3.1) - (3.2). The obtained results are reported in Table 1 for point A and in Table 2 for point B.

A numerical experiment shows that the wavelet spectrum does not depend on the partition numbers in the periodic zone. In the chaotic zone also reasonably good coincidence of the wavelet spectra is observed for different n. However, an increase of power of the frequencies associated with occurring chaos is observed. In other words, it is clearly evident that the applied wavelets analysis can be viewed as a mathematical microscope. Namely, the increase of partition numbers improves a power of our microscope. The so far illustrated and discussed results allow us to formulate a conclusion that the applied FDM is convergent regarding both wavelet spectrum and the Lyapunov exponents.

	$A(s_{01},\omega_1) = A(8.6,13.4) \in \{s_0,\omega_p\}$ (periodic vibrations)	$B(s_{02},\omega_1) = B(28.7,13.4) \in \{s_0,\omega\}$ (chaotic vibrations)
n=12	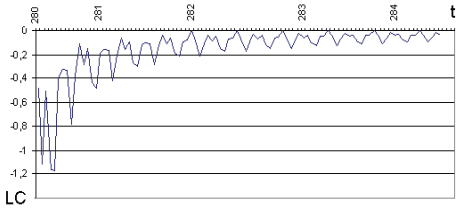	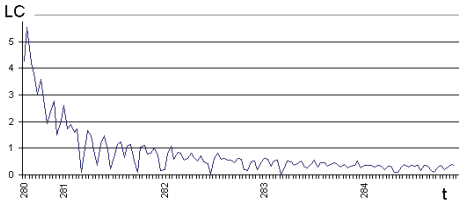
n=14	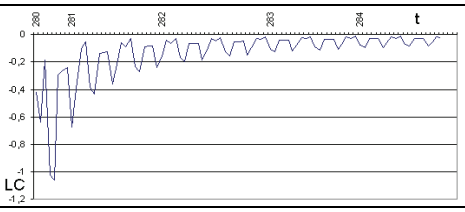	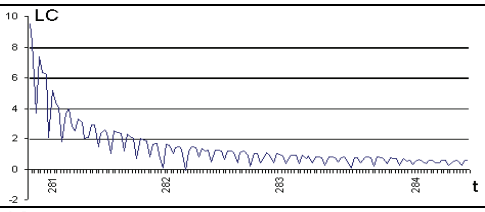
n=16	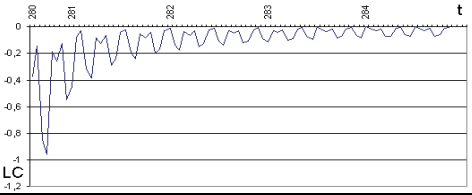	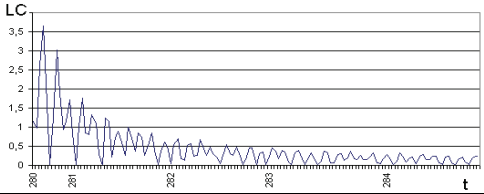

Figure 3 - The Lyapunov exponents time histories versus n in periodic and chaotic zones

Table 1 - Convergence of FDM in a periodic zone

$A(s_{01},\omega_1) = A(8.6,13.4)$	n=12	n=14	n=16
2D wavelet spectrum	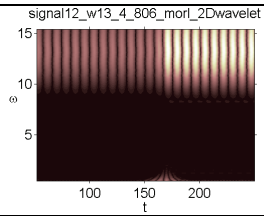	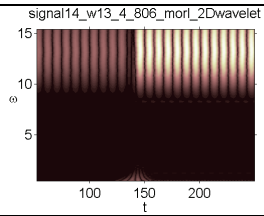	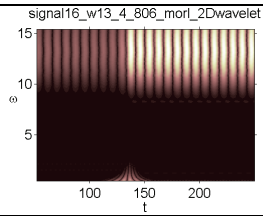
3D wavelet spectrum	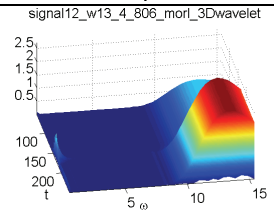	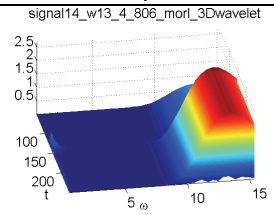	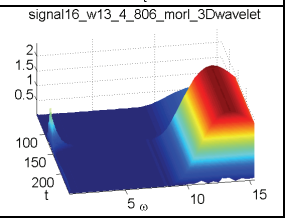

Table 2 - Convergence of FDM in a chaotic zone

$B(s_{02},\omega_1) = B(28.7,13.4)$	n=12	n=14	n=16
2D wavelet spectrum	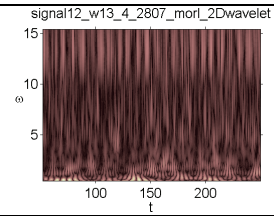	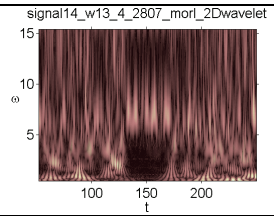	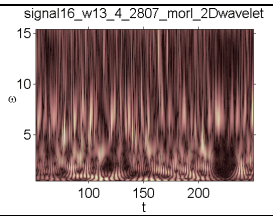
3D wavelet spectrum	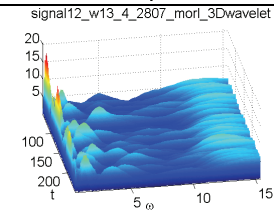	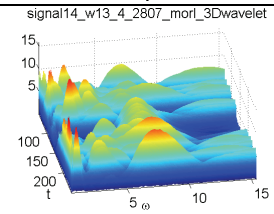	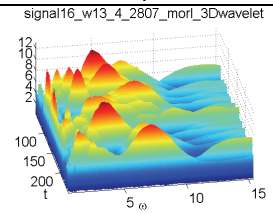

3.2. Numerical investigations

It should be emphasized that although an increase of n in the applied FDM improves essentially the obtained results, it requires an exponential increase of the computational time (one needs to solve a system of algebraic equations on each computational step, i.e. for $n = m = 8$ we have 64 equations, whereas for $n = m = 14$ we have 256 equations).

Recall that the investigations regarding the applied FDM carried out so far allow us to conclude that the numerical convergence is achieved in the average sense, i.e. with regard to the wavelet spectrum and Lyapunov exponents. In a chaotic zone the convergence with respect to the time histories is not achieved. However, in the latter case an integral convergence, i.e. with respect to the wavelet spectrum, is achieved.

Here we address another problem: is it reasonable to study only one plate point and then how to share the obtained knowledge to all plate points? In order to clarify this point we study five arbitrarily taken points of the middle plate surface with the following co-ordinates A(3;3), B(n-2; 3), C(n-2; n-2), D(3; n-2), and S(n/2; n/2) being a central middle surface point (Figure 4).

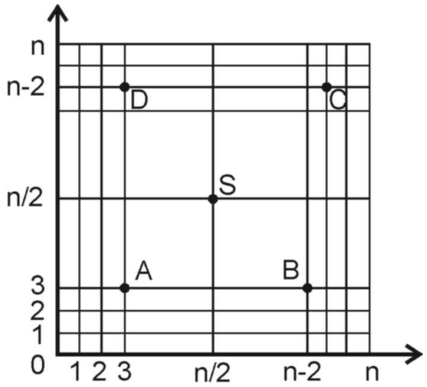

Figure 4 - Positions of points A, B, C, D, S on the middle plate surface

Analysis of each of the mentioned points is supplemented by monitoring the evolution of time-frequency characteristics of the wavelet spectra with an increase of the external load amplitude. The following external excitation frequencies have been taken into account: $\omega_p = 2.9$, $\omega_p = 5.8$ (this corresponds to natural plate vibration frequency), $\omega_p = 8.7$, and $\omega_p = 26$, $\omega_p = 13.4$. Some of the obtained results are reported in Tables 3-4. Since the frequency of compressing load has an essentially higher power in comparison to remaining frequencies, the remaining frequencies are often not visible in the wavelet spectrum owing to their small magnitudes. Therefore, our results are reported for the frequencies in a neighborhood of the excitation frequency.

Yet, it has been shown numerically that vibrations in different plate points are realized through the same frequency spectrum, although the frequencies power may differ in different points. In addition, the frequencies may vanish or reappear in time, but the spectrum record remains conserved. Consequently, it has been shown that a choice of only one plate vibration is sufficient to investigate the plate vibrations. Traditionally, we take its center as a representative point. One of the fundamental tasks of the investigation relies on monitoring a transition from regular to chaotic vibrations of our rectangular plate subjected to periodic excitation. It should be emphasized that the classical approach based on the Fourier spectrum analysis is not appropriate to detect and analyze entirely the mentioned scenarios.

Observe that while studying the plate vibrations via the Fourier analysis a few disagreements in comparison to other tested characteristics may appear. Namely, contrary to the frequency power spectrum indicating a harmonic behavior, other characteristics show the quasi-periodic dynamics. In Table 3 the following signal characteristics are reported: a time history $w(0.5;\, 0.5\, t)$ for $280 \le t \le 286$, a phase portrait $w(w'_t)$, a frequency power spectrum $S(\omega_p)$ and a Poincaré map $w_t\,(w_{t+T})$ for the center of the middle plate surface subjected to the action of load $S = s_0 \sin \omega_p t$ with the frequency $\omega_p = 5.8$ (it is equal to the plate natural vibration frequency) and with the amplitude $s_0 = 13.4$

Application of the wavelet transformation has proved that the observed differences of the signals are not accidental. On the contrary, a wavelet spectrum illustrates the fact that a transition from regularity to chaos is realized via frequencies whose power is so small that it cannot be detected using the standard Fourier analysis. In the case of excitation frequency $\omega_p = 5.8$ a scenario to chaos has been obtained via a successive period doubling bifurcation. Our wavelet analysis contradicts this statement, because the first bifurcation occurs much earlier than that reported in the Fourier spectrum (Figure 5). Figure 5 shows the first bifurcation for $\omega_1 = 2.9$, as well as the low frequency components.

Table 3 - Dynamical characteristics (ω_p = 5.8, s_0= 13.4)

	Signal $w(0.5;0.5;t)$	Phase portrait $w(w')$	Frequency power spectrum $S(\omega)$	Poincaré map $w_t(w_{t+T})$
13.4	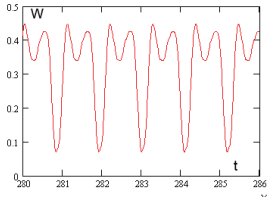	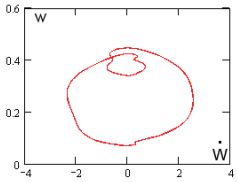	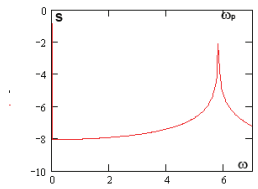	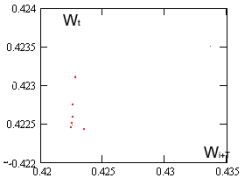

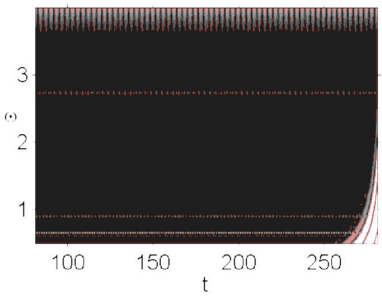

Figure 5 - Wavelet spectrum corresponding to the data of Table 3

It should be noted that during our numerical investigations with ω_p = 2.9 and ω_p = 8.7 chaotic behavior has not been detected via the classical Fourier analysis. For ω_p = 8.7 and with a small amplitude of excitation the obtained Fourier spectrum has been noisy and hence it was not possible to get a conclusion regarding the plate vibrations type. In the case of ω_p = 2.9 (Table 4), the external load amplitude increases up to 21.2 (the frequency power spectrum has indicated periodic vibrations although other dynamic characteristics have not validated this observation).

Table 4 - Scenarios of transition into chaos for ω_p = 2.9

S_0	2D wavelet spectrum	3D wavelet spectrum	S_0	2D wavelet spectrum	3D wavelet spectrum
9.1	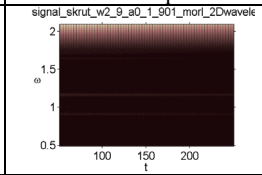	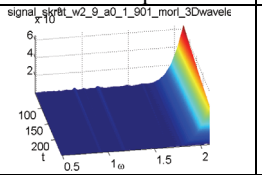	13.6	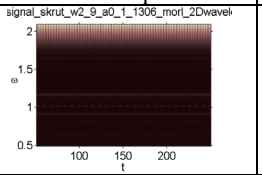	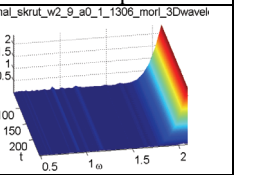
21.3	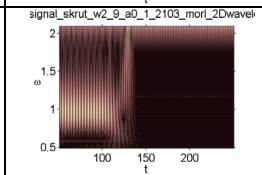	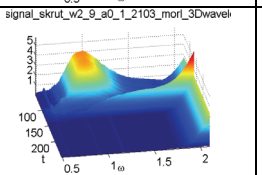	26.3	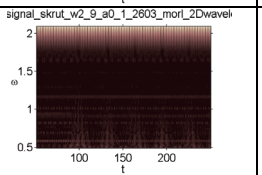	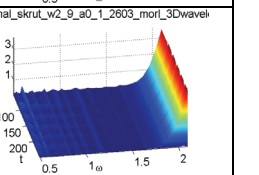
26.5	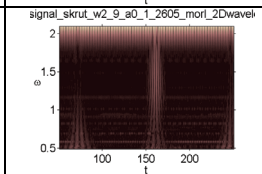	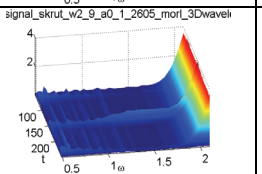	26.7	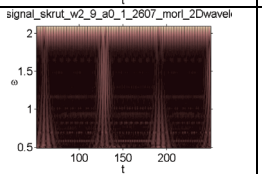	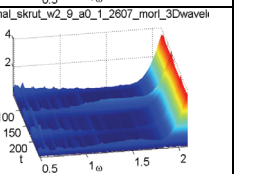
26.9	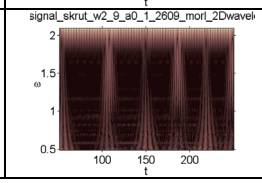	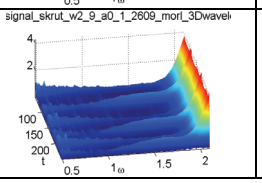	28.9	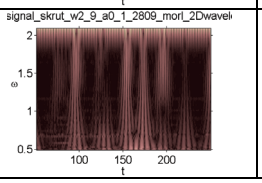	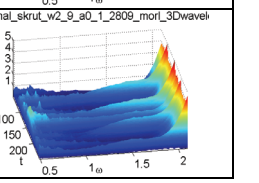

Two linearly independent frequencies ω_1 =0.9 and ω_2 = 1.15 appear in the wavelet spectrum. Their power is rather small in comparison to the excitation frequency. This is why the Fourier spectrum exhibits only a periodicity defined by external excitation. An increase of the excitation amplitude awakes a series of frequencies being combinations of ω_1 =0.9, ω_2 = 1.15 and ω_p=2.9, and for a long time the plate vibration character does not change

qualitatively. However, for s_0=21.3 a sudden doubled system reconstruction takes place in time: (i) t [50;100] – external frequency dominates and ω_1 =0.9, the observed vibrations are quasi-periodic with two non-commensurable frequencies; (ii) t [120;140] – island of chaotic transitional $s_t$ate appears; (iii) t [150;250] – the plate vibrates with three frequencies ω_p = 2.9, ω_1 = 0.9, ω_2 = 1.15.

Beginning with s_0=26.5 short transitional intermittent and periodic states are observed. The period of intermittency window is equal to 30 units, whereas the period between windows of intermittency equals 90 units. A further increase of external compressed loading amplitude causes a decrease of the period between windows of intermittency, and the plate dynamics becomes chaotic.

Since the plate transition from its regular to chaotic dynamics is associated with the occurrence of two irrational frequencies, then the illustrated scenario can be called a modified Ruelle-Takens-Newhouse scenario with intermittency in time.

4. CONCLUSIONS

Our investigations and analysis indicate that the convergence of numerically obtained results found by FDM can be achieved by monitoring a wavelet spectrum and the Lyapunov exponents. In the case of dynamics in a chaotic zone (contrary to static problems) it is impossible to achieve the convergence of time histories (signals), although one may achieve the integral convergence regarding the wavelet spectrum. In addition, in the case of small external load amplitudes one may achieve convergence with respect to signals, too. An increase of partition numbers in FDM improves the obtained results essentially, but there is a threshold value after which the results cannot be further improved. In this work we have taken n=14.

It has been explained and illustrated that frequently used FFT (Fast Fourier Transform) does not make it possible to study a continual system properly and it does not allow us either to detect and monitor transition scenarios into chaos. In other words, we have observed a lack of coincidence of the FFT results with other classical dynamical characteristics. Namely, the obtained FFT indicates the plate harmonic vibration regime, whereas the phase portrait exhibits additional frequencies. It happened because a route to chaos began on frequencies, whose power was so small that it could not be revealed by the FFT.

Furthermore, we have detected and illustrated transition scenarios from periodic to chaotic plate state, where the classical approach based on the Fourier analysis failed. In addition, we have detected and discussed two principally new scenarios. The first one is called the modified Ruelle-Takens-Newhouse scenario with intermittency, i.e. beginning with a certain value of excitation amplitude, short time periodic intervals appear. A further increase of external excitation amplitude causes a decrease of periods between intermittency windows, which finally initiates the occurrence of chaotic plate dynamics. The second scenario is associated with double dynamics reconstruction through subharmonic states before reaching chaos.

REFERENCES

[1] Awrejcewicz, J., Krysko, V.A., "Nonclassic thermo-elastic problem in nonlinear dynamics of shells", Springer- Verlag, Berlin, New York, London, Paris, Tokyo, 2003.

[2] Awrejcewicz, J., Krysko, V.A., Krysko, A.V., "Spatial – Temporal Chaos and Solutions Exhibited by Von Karman Model", International Journal of Bifurcations and Chaos, (12) 7, 2002, pp.1465-1513.

[3] Awrejcewicz, J., Krysko, V.A,. "Feigenbaum Scenario Exhibited By Thin Plate Dynamics", Nonlinear Dynamics, 24, 2001, pp.373-398.

[4] Awrejcewicz, J., Krysko, A.V., "Analysis of Complex Parametric Vibrations of Plates and Shells Using Bubnov – Galerkin Approach", Archive of Applied Mathematics, 73, 2003, pp.495-504.

[5] Awrejcewicz, J., Krysko, V.A., Vakakis, A.F., "Nonlinear dynamics of continuous elastic systems", Springer-Verlag, Berlin, New York, London, Paris, Tokyo, 2004.

[6] Yen-Liang Yeh, Chao's-Kuang Chen, Hsin-Xila, "Chaotic and Bifurcation Dynamics of a Simple-Supported Thermo-Elastic Circular Plate With Variable Thickness in Large Deflection", Chaos, Solitons and Fractals, 15(5), 2003, pp.811-829.

[7] Jones, R.M., "Buckling of bars, plates and shells", Bull Ridge Publishing, Blacksburg, Virginia, 2006.

[8] Wang, Y., "Bifurcation and Chaos of Bimetallic Circular Plates Subjected to Periodic Heat Load", Z. Angew. Math. Mech., 88(4), 2008, pp.256-266.

[9] Hao, Y.X., Chen, L.M., Zhang, W., Lei. I.G., "Nonlinear Oscillations, Bifurcations and Chaos of Functionally Graded Materials Plate", Journal of Sound and Vibration, 312(4-5), 2008, pp. 862-892.

[10] Zhang, W., "Global and Chaotic Dynamics for a Parametrically Excited Thin Plate", Journal of Sound and Vibration, 239(5), 2001, pp. 1013-1036.

[11] Sun, Y.X., Zhang, S.Y., "Chaotic Dynamics of Viscoelastic Plates", International Journal of Mechanical Sciences, 43(5), 2001, pp. 1195-1208.